

Ultrasmall TPGS–PLGA Hybrid Nanoparticles for Site-Specific Delivery of Antibiotics into *Pseudomonas aeruginosa* Biofilms in Lungs

Feng Wan,[†] Søren S.-R. Bohr,^{‡,§} Sylvia Natalie Klodzińska,[†] Haidar Jumaa,[†] Zheng Huang,[†] Tommy Nylander,^{||} Mikkel Boas Thygesen,^{‡,§} Kasper Kildegaard Sørensen,^{‡,§} Knud Jørgen Jensen,^{‡,§} Claus Sternberg,[⊥] Nikos Hatzakis,^{*,‡,§} and Hanne Mørck Nielsen^{*,†,§}

[†]Department of Pharmacy and [#]Center for Biopharmaceuticals and Biobarriers in Drug Delivery, Department of Pharmacy, University of Copenhagen, Universitetsparken 2, DK-2100 Copenhagen Ø, Denmark

[‡]Department of Chemistry & Nano-Science Center, University of Copenhagen, Thorvaldsensvej 40, DK-1871 Frederiksberg C, Denmark

[§]Novo Nordisk Foundation Centre for Protein Research, Faculty of Health and Medical Sciences, University of Copenhagen, Blegdamsvej 3B, 2200 Copenhagen, Denmark

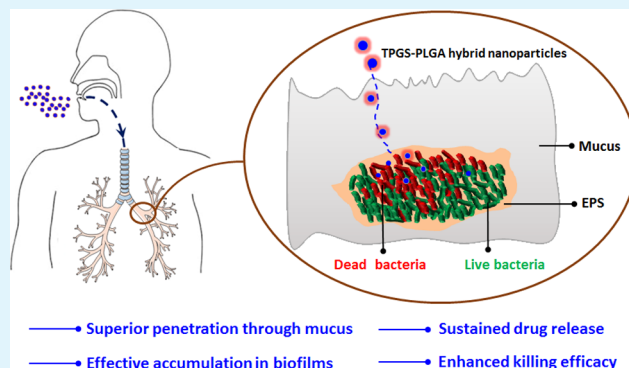
^{||}Department of Physical Chemistry, Lund University, SE-221 00 Lund, Sweden

[⊥]Department of Biotechnology and Biomedicine, Technical University of Denmark, Building 221, Søtofts Plads, DK-2800 Lyngby, Denmark

Supporting Information

ABSTRACT: Inhaled antibiotic treatment of cystic fibrosis-related bacterial biofilm infections is challenging because of the pathological environment of the lungs. Here, we present an “environment-adaptive” nanoparticle composed of a solid poly lactic-co-glycolic acid (PLGA) core and a mucus-inert, enzymatically cleavable shell of D- α -tocopheryl polyethylene glycol 1000 succinate (TPGS) for the site-specific delivery of antibiotics to bacterial biofilms via aerosol administration. The hybrid nanoparticles with ultrasmall size were self-assembled via a nanoprecipitation process by using a facile microfluidic method. The interactions of the nanoparticles with the biological barriers were comprehensively investigated by using cutting-edge techniques (e.g., quartz crystal microbalance with dissipation monitoring, total internal reflection fluorescence microscopy-based particle tracking, in vitro biofilm model cultured in a flow-chamber system, and quantitative imaging analysis). Our results suggest that the mucus-inert, enzymatically cleavable TPGS shell enables the nanoparticles to penetrate through the mucus, accumulate in the deeper layer of the biofilms, and serve as sustained release depot, thereby improving the killing efficacy of azithromycin (a macrolide antibiotic) against biofilm-forming *Pseudomonas aeruginosa*. In conclusion, the ultrasmall TPGS–PLGA hybrid nanoparticles represent an efficient delivery system to overcome the multiple barriers and release antibiotics in a sustained manner in the vicinity of the biofilm-forming bacteria.

KEYWORDS: TPGS–PLGA hybrid nanoparticles, aerosol administration, cystic fibrosis, *Pseudomonas aeruginosa* biofilm, bio–nano interaction



INTRODUCTION

Chronic *Pseudomonas aeruginosa* infection is characteristic of cystic fibrosis (CF), which usually leads to accelerated morbidity and mortality of CF patients.^{1,2} Antibiotic treatment is a cornerstone of CF therapy to reduce bacterial load, exacerbation rates, and loss of pulmonary function. However, the formation of persistent bacterial biofilms challenges the conventional antibiotic treatments that rely on parenteral and oral administration because the minimal inhibitory concentration (MIC) and the minimal bactericidal concentration of

an antibiotic to biofilm-growing bacteria can be 100–1000 fold higher than to planktonic bacteria.³ Aerosol administration of antibiotics potentially provides high drug concentration at the site of infection and minimizes systemic side effects.^{4–6} However, the abnormally thick and viscous mucus layer in CF patients hinders the diffusion of inhaled antibiotics into the

Received: November 1, 2019

Accepted: December 5, 2019

Published: December 5, 2019

regions with high bacterial loads,^{7,8} consequently, resulting in limited efficacy. In addition, extracellular polymeric substances (EPS) produced by bacteria and composed of exopolysaccharides, proteins, enzymes, lipids, and nucleic acids present a cohesive, three-dimensional polymer network that can impede the penetration of drugs into the biofilm.⁹ Furthermore, the EPS matrix may also act as an external degradative system, enabling the deactivation of antibiotics through binding interactions in these environments.¹⁰

Nanoparticle-based delivery strategies are being explored to promote the delivery of antibiotics into bacterial biofilms.^{11,12} In general, the nanoparticle size plays an important role in overcoming the steric hindrance of mucus and EPS.^{13,14} As reported, the 3D mesh spacing of fresh, undiluted, and unaltered CF sputum is in the range of 60–300 nm.¹⁵ Nanoparticles with size less than 100 nm seem to be optimal for biofilm penetration.¹⁴ In addition, a variety of surface-engineered nanoparticles has been developed to reduce the adhesive interaction of nanoparticles with mucus. In recent works, pH-sensitive polymeric nanoparticles with surface charge-switching property (i.e., presenting negatively charged surfaces at physiological condition, however, switching the surface to positive charge when exposed to bacterial infection-related acidic pH levels) demonstrated great potential for targeting delivery of antibiotics to the sites of infections via systemic administration.^{16–18} In spite of the great promise demonstrated at the tissue level (i.e., in vitro cultured bacterial biofilms), the surface charge-adaptive approach based on pH-sensitive polymers may be not applicable for aerosol antibiotics delivery due to the complicated microenvironment in lungs of CF patients, such as the acidic pH level (approximately 5.5–6.5) and the elevated salt concentration of lung lining fluid.^{19–22} For example, the pH-sensitive polymeric nanoparticles could switch their charge prior to reaching to the bacterial biofilms, consequently, leading to the mistargeting of the nanoparticles. So far, the effective approach for site-specific delivery of antibiotics into CF-related biofilms via aerosol administration is highly unmet and rarely reported.

Here, we present an environment adaptive nanoparticle delivery system by exploiting the amphiphilic structure and enzymatic cleavage of D- α -tocopheryl polyethylene glycol 1000 succinate (TPGS). TPGS is an FDA-approved pharmaceutical excipient consisting of a lipophilic moiety (vitamin E) and a hydrophilic moiety (PEG chain),^{23,24} which is documented to be cleaved into vitamin E and PEG by enzymes (e.g. esterase).²⁵ It is known that both clinical and environmental *P. aeruginosa* strains are able to produce a large array of extracellular enzymes, including esterase.^{26,27} Therefore, we expect that nanoparticles with a TPGS shell (with the PEG chain exposed toward the aqueous bulk phase) could allow the nanoparticles to penetrate through the biological barriers (e.g. mucus, EPS) into bacterial biofilms due to the low nonspecific binding of PEG.^{13,28} Subsequently, the enzymatic cleavage of TPGS in the biofilms could generate a lipophilic surface (vitamin E) of the nanoparticles, which enables the nanoparticles to anchor in the biofilm and serve as antibiotic depots, thus prolonging the exposure time of bacteria to antibiotics. To prove the concept, we fabricated TPGS–poly(lactide-co-glycolide) (PLGA) hybrid nanoparticles via the microvortex-induced nanoprecipitation process in a microfluidic chip, where the assembly of TPGS in the aqueous phase with PLGA in the organic phase results in a PLGA core surrounded by a TPGS shell with the PEG chain exposed toward the aqueous

bulk phase. In addition, we comprehensively investigated the interactions of TPGS–PLGA hybrid nanoparticles with the biological barriers (e.g. mucus, bacterial biofilm, and bacterial membrane) using a variety of cutting-edge techniques (e.g. quartz crystal microbalance with dissipation monitoring (QCM-D), total internal reflection fluorescence microscopy (TIRFM)-based particle tracking, and in vitro biofilm model cultured in a flow-chamber system, and quantitative imaging analysis). Ultimately, azithromycin (AZI, a macrolide antibiotic), which has previously demonstrated pleiotropic effects on *P. aeruginosa*,²⁹ was used to demonstrate the nanoparticle-mediated antibiofilm efficacy.

■ EXPERIMENTAL SECTION

Materials. PLGA (Resomer RG503H, L/G ratio of 50:50, molecular weight 24 000–38 000 Da), TPGS, mercaptoundecanoic acid (MUA), N-hydroxysuccinimide (NHS), N-(3-dimethylamino-propyl)-N'-ethylcarbodiimide hydrochloride (EDC), ethanolaniline hydrochloride (ETA-HCl), 11-porcine stomach mucin (type III, bound sialic acid 0.5–1.5%, partially purified powder), Mueller Hinton broth, LB broth, deoxyribonucleic acid from fish sperm, glucose, crystal violet, ethanol (HPLC grade), acetonitrile (HPLC grade), sodium phosphate monobasic (NaH₂PO₄), sodium chloride (NaCl), citric acid, 4-(2-hydroxyethyl)-1-piperazineethanesulfonic acid (HEPES), and tris(hydroxymethyl)aminomethane (Tris) were purchased from Sigma-Aldrich (Broendby, Denmark). 1,1'-Dioctadecyl-3,3,3',3'-tetramethylindocarbocyanine perchlorate (DiIC₁₈₍₃₎) and propidium iodide (PI) were purchased from Invitrogen (Carlsbad, CA, USA) and Molecular Probes (Eugene, OR, USA), respectively. 1-Palmitoyl-2-oleoyl-*sn*-glycero-3-phosphoethanolamine (POPE) and 1-palmitoyl-2-oleoyl-*sn*-glycero-3-phospho-(1'-rac-glycerol) (POPG) were purchased from Avanti Polar Lipids (Alabaster, AL, USA). AZI dihydrate (97%) was bought from Fluorochem (Hadfield, UK). *P. aeruginosa* (PA O1) and *P. aeruginosa* (PAO1 tagged with GFP) were kindly provided by the Institute of Immunology and Microbiology (University of Copenhagen) and the Department of Biotechnology and Biomedicine (Technical University of Denmark), respectively. Ultrapure water was obtained from a PURELAB flex machine (ELGA LabWater, High Wycombe, UK).

Preparation and Characterization of Nanoparticles. TPGS–PLGA hybrid nanoparticles were prepared by using a microfluidic method as previously reported.³⁰ Briefly, the organic phase, composed of 1% (w/v) PLGA in acetonitrile, and the aqueous phase, composed of TPGS (0.01–0.2%, w/v) in HEPES buffer (10 mM, pH 7.4) (without TPGS for preparation of PLGA nanoparticles) were pumped by using syringes (Gastight 1010, Hamilton Robotics, Reno, NV, USA) into the inner channel (flow rate 1 mL/min) and outer channels (5 mL/min) of the microfluidic chip, respectively. The resulting nanoparticle dispersion was collected in a beaker and stored in a dark room under magnetic stirring for 4 h to evaporate the organic solvent.

For the preparation of the fluorescent nanoparticles for the investigation of mucus-penetrating property using particle tracking, Atto655-conjugated PLGA was synthesized (Supporting Information, Figures S1 and S2) and used to label the nanoparticles by the addition of Atto655-conjugated PLGA (2% w/w to PLGA) to the organic phase. For the preparation of the fluorescent nanoparticles for the investigation of the nanoparticle penetration into the bacterial biofilms, DiIC₁₈₍₃₎ was added to the organic phase to a final concentration of 0.005% (w/v). For the preparation of antimicrobial nanoparticles (AZI-loaded TPGS–PLGA hybrid nanoparticles), AZI was dissolved in the organic phase to the concentration of 0.2% (w/v). The unencapsulated AZI was then removed by centrifugation (4000g) using an Amicon filter (MWCO 100 kDa, Merck, Darmstadt, Germany).

Size and zeta potential of the nanoparticles were measured by using dynamic light scattering and laser Doppler electrophoresis,

respectively. The samples were diluted using HEPES buffer (10 mM, pH 7.4) to a concentration of 0.1 mg/mL prior to measurements, which were carried out at 25 °C by using a Zetasizer Nano ZS (Malvern Instruments, Worcestershire, UK) equipped with a 633 nm laser and 173° detection optics. Data acquisition and analysis were performed by using the Malvern DTS v6.30 software (Malvern Instruments). The morphological analysis of the nanoparticles was carried out by using a Tecnai G2 20 TWIN transmission electron microscope (FEI, Hillsboro, OR, USA). The nanoparticle sample in ultrapure water (100 μ L) was mounted onto a transmission electron microscopy (TEM) grid, followed by staining with 1% (w/v) ammonium molybdate for 1 min. The grid was dried by removing the liquid using a filter paper. All of the observations were made in the bright field mode at an acceleration voltage of 10 kV. The digital images were recorded with a Gatan Imaging Filter 100 CCD camera (Gatan, Pleasanton, CA, USA).

Encapsulation Efficiency, Drug Loading, and Drug Release.

To determine the drug loading and the encapsulation efficiency of AZI in the nanoparticles, the purified AZI-loaded TPGS–PLGA hybrid nanoparticles in suspension (50 μ L) were dissolved in acetonitrile (250 μ L). The amount of AZI, TPGS, and PLGA were analyzed by using high-performance liquid chromatography with an evaporative light scattering detector (ELSD–HPLC) (Supporting Information, Table S1, and Figure S3). The average encapsulation efficiency (EE %) and the drug loading (DL %) were calculated by using eqs 1 and 2, respectively

$$EE \% = \frac{m_{AZI}}{M_{AZI}} \times 100\% \quad (1)$$

$$DL \% = \frac{m_{AZI}}{m_{AZI} + m_{PLGA}} \times 100\% \quad (2)$$

where EE % is the encapsulation efficiency; DL % is the drug loading of AZI into nanoparticles; M_{AZI} is the amount of AZI in the nonpurified nanoparticles dispersion, m_{AZI} is the content (mass) of AZI in the purified nanoparticles; m_{PLGA} is the content (mass) of PLGA in the purified nanoparticles.

In vitro drug release of AZI from the nanoparticles was investigated by using a dialysis-bag method. Briefly, 1 mL of AZI-loaded TPGS–PLGA hybrid nanoparticle dispersion (with a total drug concentration of 500 μ g/mL) was transferred into dialysis cassettes (MWCO 100 kDa, Thermo Fisher Scientific, Waltham, MA, USA). As a control, 1 mL of AZI solution (500 μ g/mL) in HEPES buffer (pH 7.4) was injected into a separate dialysis cassette. The cassettes were then immersed into a 4 mL reservoir of HEPES buffer solution (pH 7.4) in an incubator at 37 °C, with shaking using a linear shaking bath system (GLS400, Grant Instruments, Germany). The release medium was replaced with 4 mL of fresh HEPES buffer solution (pH 7.4) at predetermined time intervals. The amount of drug in the collected release medium was assayed by using an HPLC method.

TIRFM-Based Particle Tracking. Particle tracking experiments were performed using a total internal reflection fluorescence microscope (IX 83, Olympus, Tokyo, Japan) using a EMCCD camera (ImagEM X2, Hamatsu, Hamamatsu City, Japan) and an oil immersion 100 \times objective (UAPON 100XOTIRF, Olympus, Tokyo, Japan), resulting in a resolution of 160 nm per pixel. Atto655-labeled PLGA nanoparticles were excited using a 655 nm solid state laser line (Cellsens, Olympus, Tokyo, Japan) with an exposure time of 50 ms, 200 nm penetration depth, and 300 EM gain. A 700/75 nm ET band pass filter was used to filter the emission signal. All experiments were performed at 37 °C. The TIRFM setup allows for real-time monitoring of individual particle characteristics and behaviors in close proximity to the surface (i.e., evanescent plane) by eliminating signals from the bulk sample.

Penetration Experiments. To measure the rate of nanoparticle penetration, 20 μ L of biosimilar mucus prepared as described previously³¹ (pH 6.5) was added to a custom-built Teflon chamber designed to support \varnothing 25 microscopy glass slides, resulting in a mucus layer of approximately 2 mm. The nanoparticles were mixed with mucus in a 1:10 ratio (v/v) to (a) dilute the nanoparticle dispersion

and to (b) avoid further dilution of the mucus within the chamber upon the addition of the sample. The freshly prepared mucus–nanoparticle dispersion was vortexed and allowed to equilibrate 10 min at 37 °C prior to imaging. Subsequently, the image acquisition was initiated once the mucus–nanoparticle dispersion (15 μ L) was carefully added on top of the mucus layer in the chamber. The imaging at the deposition surface was recorded at a frame rate of 1 s^{−1}, enabling long-term experiments and thus extraction of arrival times through the mucus.

Tracking Experiments. To further investigate the interaction of nanoparticles with mucus and bacterial membranes, we set up an assay to track the movement of single particles at the interface between mucus and the bacterial membrane. Prior to imaging, a mixture of nanoparticle and mucus was made as described above and after equilibration added to a microscopy chamber (total dispersion volume of 20 μ L). Image acquisition was performed to record the ultra-fast behavior at a frame rate of 15.2 s^{−1}. To investigate the nanoparticles interaction with the bacterial membrane, the glass slide of the microscopy chamber was coated with a lipid bilayer composed of POPE and POPG (3:1, molar ratio) by using the previously reported approach,³² which is usually used for mimicking the outer membrane of *P. aeruginosa*.³³ The diffusion parameters of the nanoparticles were obtained by analyzing the moving trajectory of the nanoparticles at the interface between mucus and the bacterial membrane.

Image Analysis. Quantitative image analysis was performed using a combination of the ImageJ plugin TrackMate (for localization of particles) and custom routines developed in-house using R and Python.³⁴ Particles were located in the *xy*-plane using a Laplacian of Gaussian approach,^{35,36} which allows sub-pixel localization and tracking. For both penetration experiment and diffusion experiment, only particles residing in the observable zone for 10 frames or more would be used for analysis. To avoid the introduction of falsely connected particles, a maximum distance (step size) between consecutive frames of 0.96 μ m was applied. The setup of the penetration experiment, due to the low frame rate, allows for the long-term measurements (>40 min) of particles arriving at the evanescent field (observable zone), thus directly providing a correlation to time of penetration. However, during the penetration experiments, particles cannot be tracked individually and thus the number of arrived particles was counted instead. In addition, to further decipher the interaction of the nanoparticles with the mucus, a spatial analysis of particle density is conducted by using the Ripley's K function (Supporting Information, Figure S4).³⁷ For the tracking experiments, the mean square displacement (MSD) of each individual particle was calculated as earlier shown^{38,39}

$$\begin{aligned} \text{MSD} (\tau = n \times \Delta t) \\ = \langle r^2(\tau) \rangle \times \frac{1}{N-n} \times \sum_{i=1}^{N-n} (x_{i+n} - x_i)^2 + (y_{i+n} - y_i)^2 \end{aligned} \quad (3)$$

where Δt is the time interval, N is the number of total frames, and x_i and y_i are coordinates at $t = i$. From the MSD, the instantaneous diffusion coefficient was calculated by fitting a straight line to the initial lag times.⁴⁰

Quartz Crystal Microbalance with Dissipation Monitoring. QCM-D measurements were performed with an E4 system from Q-Sense (Gothenburg, Sweden) using carboxylic acid-functionalized, gold-coated quartz crystals with a fundamental frequency of 4.95 Hz (QSX301, Q-Sense). To deposit a stable mucin layer on the crystals, mucin was immobilized on the crystals by using an amine-coupling method. Briefly, the crystals were first functionalized with a monolayer of carboxylic acid by immersing in a 1 mM ethanolic solution of MUA for at least 12 h at room temperature. The resulting functionalized gold-coated quartz crystals were subsequently rinsed with ethanol, dried, and mounted in the QCM-D chamber. While mounted in the chamber, the crystals were exposed to an aqueous solution of 200 mM EDC and 50 mM NHS for 10 min, followed by rinsing with ultrapure

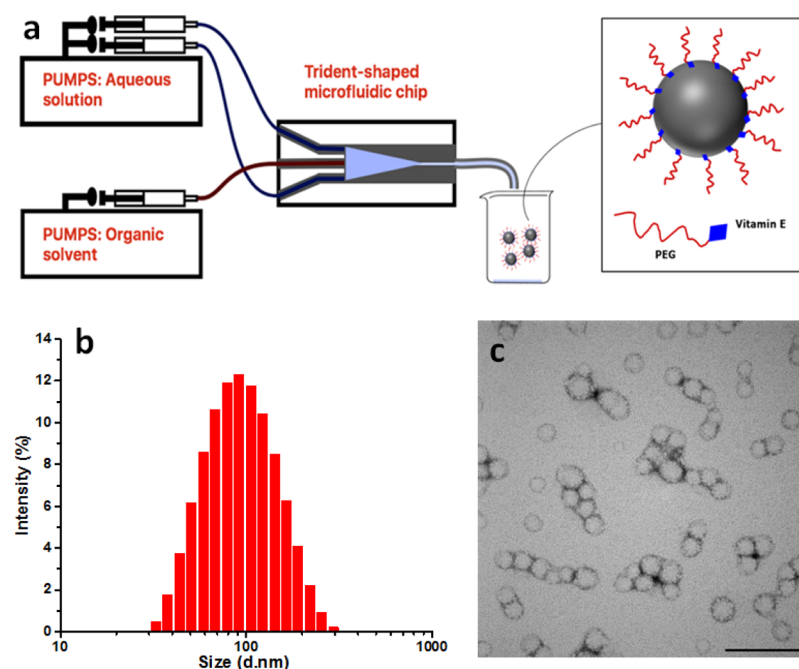


Figure 1. (a) Schematic illustration of preparation and structure of TPGS–PLGA hybrid nanoparticles prepared by using the microfluidic method; (b) representative size distribution by intensity of TPGS–PLGA hybrid nanoparticles (type F, Table S3); and (c) TEM image of AZI-loaded TPGS–PLGA hybrid nanoparticles (type D, Table S4). Scale bar: 200 nm.

water and citrate buffer (10 mM, pH 4.0). Afterward, 0.5 mg/mL mucin in citrate buffer was applied for 30 min, followed by rinsing with the citrate buffer for 10 min. Unreacted NHS-ester was deactivated by rinsing with 1 M ETA-HCl (in Tris buffer, 10 mM, pH 8.5) for 15 min. Following another rinsing with phosphate buffer (PBS, pH 6.25, ionic strength 150 mM) for 10 min, nanoparticle dispersions in PBS (pH 6.25, ionic strength 150 mM) were applied in the QCM-D chamber, and changes in frequency (Δf) and energy dissipation factor (ΔD) were simultaneously recorded. All experiments were conducted at 37 °C and at a constant flow rate of 50 $\mu\text{L}/\text{min}$. QCM-D measurements were performed in least triplicate, and representative measurements are presented.

Exposure of the Biofilm to Fluorescent and Antimicrobial Nanoparticles in a Flow Chamber System. *Cultivation.* Biofilms of *P. aeruginosa* were grown in a flow-chamber system containing individual channels with the dimensions of $1 \times 4 \times 40$ mm, as described previously.⁴¹ Each channel of the flow-chamber was inoculated with 300 μL aliquots of overnight cultures of *P. aeruginosa* (PAO1 tagged with GFP), which were pregrown in the LB medium at 37 °C under vigorous shaking and adjusted to an optical density of 0.001 at 600 nm by using 0.9% NaCl solution. After inoculation, the flow channels were left without flow for 1 h at 37 °C to allow adhesion of the bacterial cells to the substratum, after which the growth medium with 0.3 mM glucose (Supporting Information, Table S2) was supplied at a flow rate of 3 mL/h by using a peristaltic pump (Watson-Marlow 205S, Watson-Marlow, Cornwall, UK). The flow-chamber system was incubated at 37 °C for 3–4 days until the biofilms were ready for the following investigation.

Nanoparticle Penetration. To investigate the penetration of nanoparticles into the biofilms cultivated in the flow-chamber channels, each channel of the flow-chamber system was gently dosed with 300 μL aliquots of fluorescent nanoparticles (DiIC18(3)-labeled PLGA nanoparticles and DiIC18(3)-labeled TPGS–PLGA hybrid nanoparticles), after which the system was left without flow for 30 min at 37 °C. Subsequently, the 3 mL/h flow of the growth medium with 0.3 mM glucose (Supporting Information, Table S2) was resumed. The penetration of fluorescent nanoparticles into the biofilms was observed at predetermined time intervals. To quantify the nanoparticles residing within the bacterial biofilm, the confocal laser scanning microscopy (CLSM) images (confocal z-stack) were

first split into a bacterial channel and a nanoparticle channel. Subsequently, applying a Gaussian smoothing factor to each slice, a mask was created using a hard threshold of 1.5 times the standard deviation of the image. This mask was applied to the nanoparticle channel to extract signal and hence avoid nonspecifically bound nanoparticles. Additionally, the mask allowed us to correct for the total amount of biofilm measured and hence provide normalized and comparable data between nanoparticles in an otherwise heterogeneous system.

Killing Efficacy. To investigate the killing efficacy of the antimicrobial nanoparticles (AZI-loaded TPGS–PLGA hybrid nanoparticles) against the biofilms, each channel was gently dosed with 300 μL aliquots of antimicrobial nanoparticles (corresponding to a total of 1 mg/mL of AZI) and the system equilibrated as described above. To differentiate dead and live cells, PI (dead cell indicator) was added to the medium at a final concentration of 0.3 mM.⁴² The dead and live cells in the biofilms were visualized at predetermined time intervals. To quantify the amount of dead bacteria present in the bacterial biofilm, the following method was applied. Each image was split in a living biofilm channel (green) and a channel containing the dead bacteria (red), respectively. To ensure correct quantification and comparison of the killed bacteria residing in the biofilm, a mask was created using the signal from both live and dead biofilm combined. The mask was created by applying sequentially to each slice in the z-stack (a) a Gaussian smoothing factor and (b) hard threshold of 1.5 times the standard deviation of the given slice. By using the total integrated signal from the dead bacteria (red channel) and normalizing to the amount of biofilm measured, we were able to provide a relative killing efficiency difference between investigated nanoparticles. The killing efficiency was defined as follows

$$K_e = \frac{1}{n} \sum_0^n \left(\frac{1}{V_{B,n}} \sum_0^m S_{D,m} \right) \quad (4)$$

where K_e is the killing efficiency corrected for the amount of biofilm measured, n is the number of images in a given experiment, V_B is the total volume of biofilm in image n , m is the number of z-stacks in n , and S_D is the signal from the dead bacterial biofilm in slice m .

Visualization. The biofilms, nanoparticle penetration, and killing efficiency were visualized by using a confocal laser scanning

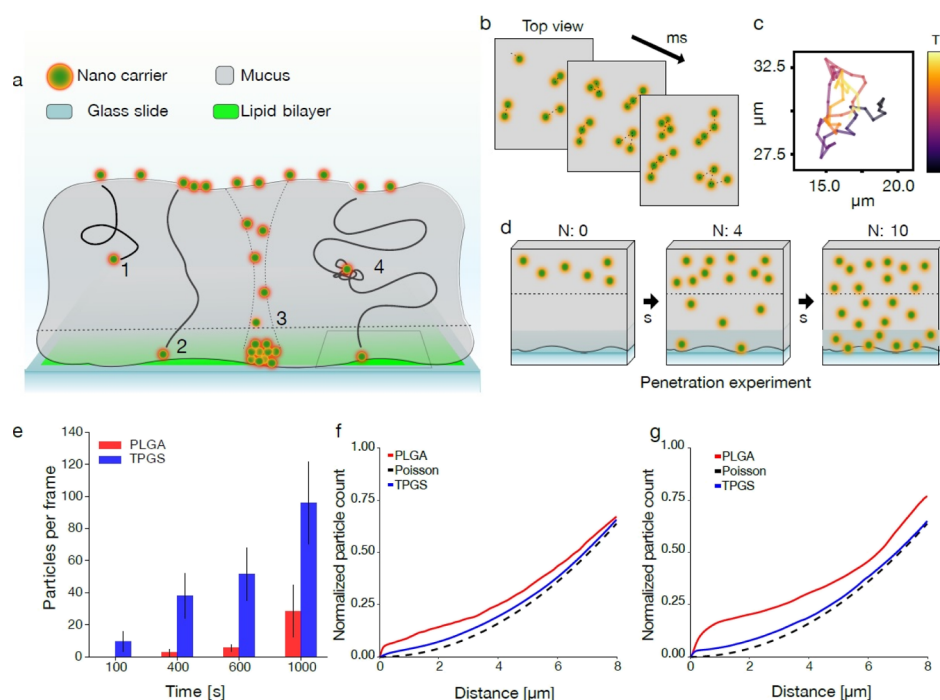


Figure 2. (a) Cartoon illustration of nanoparticles penetrating through a mucosal layer placed on top of a microscope glass slide and visualized by using TIRFM. Dashed line indicates observable zone, determined by the penetration depth used during acquisition (200 nm). Number 1, 2, 3, and 4 represent the distinct behaviors of nanoparticles in the mucus. Only the nanoparticles entering the observable zone can be analyzed; (b) schematic illustration of TIRFM-based particle tracking with high temporal resolution allowing linking of distinct particles in time (tracking experimental setup); (c) representative moving trajectory of a single nanoparticle. Color code indicates the observation time; (d) schematic illustration of TIRFM-based particle tracking with a low frame rate allowing long-term measurements (>40 min) of the total number of nanoparticles per frame (penetration experimental setup); (e) time-dependent number of detected particles per frame (as displayed in (d)); (f) spatial localization pattern of nanoparticles after 20 min; and (g) spatial localization pattern of nanoparticles after 40 min. Red: PLGA nanoparticles (type I, Table S3); blue: TPGS–PLGA hybrid nanoparticles (type J, Table S3).

microscope (Zeiss LSM 510, Carl Zeiss, Germany) equipped with detectors and filter sets for monitoring of GFP (excitation, 488 nm; emission, 517 nm), DiIC₁₈₍₃₎, and PI (excitation, 543 nm; emission, 565 nm). Images were obtained using a 40×/1.3 Plan-Neofluar oil immersion objective. Simulated 3D images and multichannel cross sections were generated using the Imaris software package (version 9.2) (Bitplane, Zürich, Switzerland).

RESULTS AND DISCUSSION

Nanoparticle Preparation and Characterization.

TPGS–PLGA hybrid nanoparticles were synthesized via microvortex-induced rapid mixing of a PLGA organic solution in the inner channel with an aqueous solution containing TPGS in the outer channels by using a three-inlet microfluidic chip, as described previously.³⁰ The use of microvortices enables up to 1000 times higher productivity than the conventional microfluidic methods based on diffusive mixing and convective mixing, thus facilitating good manufacturing practice production and clinical translation of nanoparticle-based formulations.³⁰ The microvortex pattern can be regulated by varying the Reynolds number (Re) and the flow rate ratio of the inner organic solution to the outer aqueous solution. The previous studies demonstrated that the flow rate ratio of 1:10 and the Re of 150 can ensure high performance of nanoparticle synthesis.^{43,44} Hence, these parameters were used in the present study for the synthesis of TPGS–PLGA hybrid nanoparticles and resulted in the formation of nanoparticles with a size of less than 100 nm (Figure 1 and Supporting Information, Table S3). Langer and co-workers have previously shown that the formation of lipid–PLGA hybrid

nanoparticles in the microfluidic-based one-step method indeed involves two distinct stages occurring within a very small time scale: (i) formation of a PLGA core via the self-assembly of PLGA molecules owing to the solvent displacement and (ii) lipid shell formation as soon as the lipid molecules assemble to the surface of the formed PLGA cores.⁴⁴ To investigate the role of TPGS on the self-assembly of the nanoparticles, we investigated to what extent the self-assembly of PLGA was affected by the presence of TPGS. The increase in the concentration of TPGS from 0.1 to 0.5 mg/mL decreased the nanoparticle size from 81 to 67 nm. However, a further increase in the concentration of TPGS to 2 mg/mL resulted in an increased size, which could be because the elevated viscosity of the inner aqueous solution with the increasing TPGS concentration decreased the mixing efficiency. Additionally, the increase in the concentration of TPGS led to less negative zeta potentials from -48 to -28 mV, which is indicative of the self-assembly of TPGS molecules on the surface of nanoparticles. The fluorescent nanoparticles with comparable sizes and zeta potentials were obtained by incorporating Atto655-conjugated PLGA or DiIC₁₈₍₃₎ into PLGA nanoparticles and TPGS–PLGA hybrid nanoparticles (Supporting Information, Table S3). Interestingly, it was observed that the encapsulation of AZI into the nanoparticles resulted in a smaller nanoparticle size (Supporting Information, Table S4), which is supported by the TEM images (Figure 1c), though the mechanism is still unclear. In general, an average EE % of AZI between 14 and 24% was obtained (Supporting Information, Table S4) and can be slightly

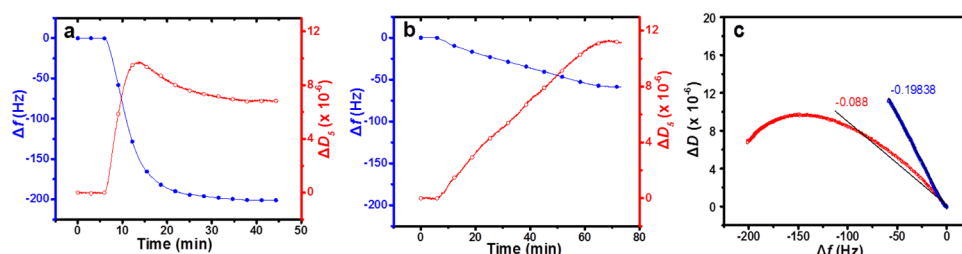


Figure 3. (a) Representative QCM-D measurements of the changes in frequency (Δf , blue) and energy dissipation factor (ΔD , red) upon the interaction of PLGA nanoparticles (type A, Table S3) with a mucin layer at pH 6.25, ionic strength 150 mM; (b) TPGS–PLGA hybrid nanoparticles (type F, Table S3) with a mucin layer at pH 6.25, ionic strength 150 mM; (c) ΔD – Δf plots of adsorption of PLGA nanoparticles (red) and TPGS–PLGA nanoparticles (blue) onto a mucin layer at pH 6.25, ionic strength 150 mM.

improved by increasing the pH of the aqueous phase due to the pH-dependent solubility of AZI.⁴⁵ The increase in the pH of the aqueous solution seemingly decreased the particle size, which could be attributed to the change in pH enhancing the intermolecular interaction between AZI and the PLGA (e.g., hydrophobic interaction) during the assembly of the nanoparticles and shrinking the dimension of the nanoparticles. The difference in zeta potentials induced by the pH of the aqueous solution could be due to the different surface enrichment of AZI and the different orientation of PLGA chains in the nanoparticles. However, no effects on size and zeta potential were observed with increasing TPGS concentration in the aqueous phase from 1 to 2 mg/mL.

Penetration of Nanoparticles in Mucus. The pathologically thick and viscous mucus layer lining the airways represents one of the important barriers to efficient antimicrobial therapy because the inhaled nanoparticles may be trapped via steric immobilization and/or adhesive interaction with the components in the mucus. In both cases, the restrained diffusion of the nanoparticles in the mucus will decrease their accumulation in close vicinity of the bacterial cells and result in lower efficiency.^{3,10} Thus, for the successful delivery of antimicrobials to bacteria residing inside mucus, nanoparticles must be able to penetrate through mucus without being entrapped in the dense mucus network.

The mucus-penetrating property of the nanoparticles was investigated by using a TIRFM-based particle tracking technique. Here, we applied the principle of TIRFM-based particle tracking to record the appearance of nanoparticles, which have penetrated the mucus layer and reached the evanescent plane of 200 nm (Figure 2a–d). Thus, compared to the conventional particle tracking, this approach allows for the exclusive detection of particle penetration through a biologically relevant thickness of mucus. Direct counting of the number of particles per frame showed a time-dependent increase for both the PLGA and the TPGS–PLGA hybrid nanoparticles, reflecting the process of nanoparticle penetration across the mucus layer. Interestingly, the TPGS–PLGA hybrid nanoparticles presented a faster onset of penetration and a steeper slope of the particle number–time curve (Figure 2e) during the initial 20 min, indicative of a more superior mucus-penetrating property compared to PLGA nanoparticles. In addition, the PLGA nanoparticles showed evident penetration, which could be attributed to the ultrasmall size of PLGA nanoparticles. As reported previously, the mesh spacing of fresh, undiluted, and unaltered CF sputum ranges 60–300 nm.¹⁵ Thus, for the nanoparticles with the diameter less than 60 nm, the steric hindrance of mucus would be minimized. The difference in mucus-penetrating behaviors

between PLGA nanoparticles and TPGS–PLGA hybrid nanoparticles could mainly result from their adhesive interaction with mucus. Thus, to decipher the interaction of the nanoparticles with the mucus, a spatial analysis of particle density was conducted by using the Ripley’s K function,³⁷ which counts the average distance from a particle to its neighbors (Supporting Information, Figure S4), thus allowing one to quantitatively describe the degree of nanoparticle localization at the certain areas due to such bio–nano interactions. The spatial localization pattern showed a random distribution pattern of TPGS–PLGA hybrid nanoparticles, suggesting that TPGS–PLGA hybrid nanoparticles can effectively “slip” through the mucus in a uniform manner. On the contrary, PLGA nanoparticles tended to concentrate in the discrete areas (Figure 2f,g), indicating that PLGA nanoparticles are highly affected by spatial-discrepancy within the bio-matrix.

QCM-D measurements were further performed to evaluate the adhesive interactions between mucin and nanoparticles, as previously reported.⁴⁶ Introduction of the PLGA nanoparticles onto the preformed mucin layer representing a pathologically relevant lung condition (pH 6.25, ionic strength 150 mM) resulted in a Δf of about -200 Hz (for the fifth harmonic overtone, i.e., $n = 5$) (Figure 3a). In comparison, introduction of the TPGS–PLGA hybrid nanoparticles onto the mucin layer representing the identical pathologically relevant lung condition (pH 6.25, ionic strength 150 mM) led to a Δf of -60 Hz in 60 min (Figure 3b), suggesting much slower dynamics of adsorption of the TPGS–PLGA hybrid nanoparticles onto the mucin layer. Additionally, it was observed that the ΔD versus Δf plot of the PLGA nanoparticles showed a less steep slope than that obtained for the TPGS–PLGA hybrid nanoparticles (Figure 3c), indicating that the TPGS coating effectively reduced the stiffness of the interaction between nanoparticle and mucin. This would be attributed to the hydrophilic and less negatively charged surface of the TPGS–PLGA hybrid nanoparticles. Interestingly, upon introducing the PLGA nanoparticles onto the immobilized mucin layer, ΔD increased promptly to $\sim 10 \times 10^{-6}$ at the initial stage (within first 10 min). However, a gentle decline of ΔD (to $\sim 6 \times 10^{-6}$) was observed with the continuous adsorption of the PLGA nanoparticles (Figure 3a). This phenomenon could result from the transformation of a “soft” mucin layer to a more “rigid” layer, which is likely induced by the intensive adhesive interaction between the PLGA nanoparticles and the mucin layer. In line with the particle tracking results, these observations suggest that the TPGS coating can effectively reduce the mucin–nanoparticle interaction and improve the mucus-penetrating property of the nanoparticles.

Accumulation of Nanoparticles in Bacterial Biofilms.

The spatial location of the fluorescent nanoparticles in *P. aeruginosa* biofilms grown in a flow-chamber system under well-controlled and hydrodynamic conditions was visualized by using CLSM.⁴¹ This flow-chamber system allows for the visualization of the complex multicellular structures present in *P. aeruginosa* biofilms (e.g., mushroom-shaped biofilms)⁴⁷ and observation of nanoparticle penetration into the biofilms. In addition, the nanoparticles that do not bind to the bacterial biofilms will be removed with the hydrodynamic flow in the chambers, which is a highly relevant to an in vitro lung clearance model. This is highly advantageous compared to the conventional methodologies applying static conditions because more dynamic conditions will include the effects of shear stress and clearance.

Exposure of the heterogeneous multicellular *P. aeruginosa* biofilms with both DiIC₁₈₍₃₎-labeled PLGA nanoparticles and DiIC₁₈₍₃₎-labeled TPGS–PLGA hybrid nanoparticles resulted in the accumulation of red-fluorescent nanoparticles in green-fluorescent (GFP-tagged) *P. aeruginosa* biofilms (Figure 4a,c),

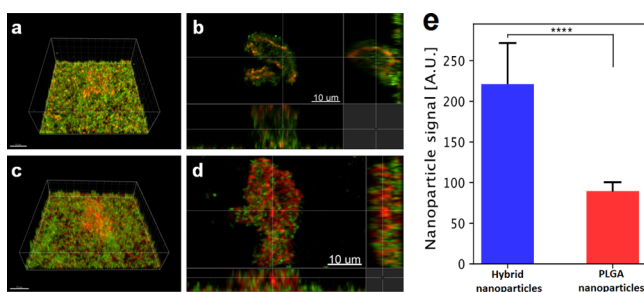


Figure 4. Penetration of DiIC₁₈₍₃₎-labeled PLGA nanoparticles (type G, Table S3) and DiIC₁₈₍₃₎-labeled TPGS–PLGA hybrid nanoparticles (type H, Table S3) in the *P. aeruginosa* biofilm (PAO1 tagged with GFP). (a,b) CLSM images of DiIC₁₈₍₃₎-labeled PLGA nanoparticles accumulated in the *P. aeruginosa* biofilm at 5 h. (c,d) CLSM images of DiIC₁₈₍₃₎-labeled TPGS–PLGA hybrid nanoparticles accumulated in the *P. aeruginosa* biofilm at 5 h. (a,c) 3D images; (b,d) 2D cross-section images (the central pictures show top–down views, and the flanking pictures show side views). *P. aeruginosa* bacteria appear green due to the expression of GFP and the fluorescent nanoparticles appear red due to labeling with DiIC₁₈₍₃₎. Scale bars: 10 μm . (e) Quantitative analysis of nanoparticles in the bacterial biofilm. Statistics by student's *t*-test: **** indicate *p*-value < 0.0001.

indicating adequate penetration of both nanoparticles into the bacterial biofilm because of their ultrasmall size (less than 100 nm, Supporting Information, Table S3). However, the

fluorescent PLGA nanoparticles appeared to primarily localize at the superficial layer of the biofilm (Figure 4b). In contrast, the fluorescent TPGS–PLGA hybrid nanoparticles were able to penetrate deeper into the central part of the biofilm (Figure 4d), suggesting superior biofilm-penetrating property of the TPGS–PLGA hybrid nanoparticles. Quantitative imaging analysis of the penetration of nanoparticles in biofilms displayed that the TPGS–PLGA hybrid nanoparticles presented approximately 2 times higher density in the bacterial biofilms compared to PLGA nanoparticles (Figure 4e). The observation indicates that the surface-enriched carboxyl groups of PLGA nanoparticles may strongly interact with and bind to the components of the EPS, thus hindering the diffusion of PLGA nanoparticles into the deeper layer of the biofilms. In contrast, the surface-enriched PEG moieties of TPGS–PLGA hybrid nanoparticles effectively display reduced interaction and binding of the nanoparticles with the components of the EPS, thus allowing for adequate penetration of the nanoparticles into the deeper layer of the biofilms.

The mobility of the nanoparticles at the interface between mucus and the bacterial membrane was investigated by using TIRFM-based particle tracking with the tracking experimental setup (Figure 2b). The glass slides in a microscopy chamber were coated with a lipid bilayer composed of POPE/POPG = 3:1. This lipid mixture mimics the charges of the outer membrane of *P. aeruginosa*³³ and is ideal for in vitro quantitative analysis of the interaction, kinetics, and diffusional properties of the two nanoparticle systems at the interface between mucus and the bacterial membrane. The high fidelity of the assay allowed for the identification and tracking of hundreds of individual nanoparticles per frame (>1000) simultaneously within a single experiment (Figure 5a) and estimation of diffusion coefficient and individual step sizes (i.e., the displacements in the position of nanoparticles between frames). Compared to PLGA nanoparticles, the TPGS–PLGA hybrid nanoparticles presented up to 5 times longer step lengths with a more heterogeneous distribution (Figure 5b) and a higher diffusion coefficient (Figure 5c), indicating the higher mobility of the TPGS–PLGA hybrid nanoparticles at the boundary between the mucus and the bacterial outer membrane-mimicking lipid bilayer. This higher mobility could, however, potentially facilitate the escape of TPGS–PLGA hybrid nanoparticles from the biofilm with the hydrodynamic flow and thus could represent a drawback to the long-term sustained delivery of antimicrobials in the biofilms.¹² However, it was observed that TPGS–PLGA hybrid nanoparticles presented a comparable retention in the biofilm after 24 h with that of PLGA nanoparticles (Supporting Information,

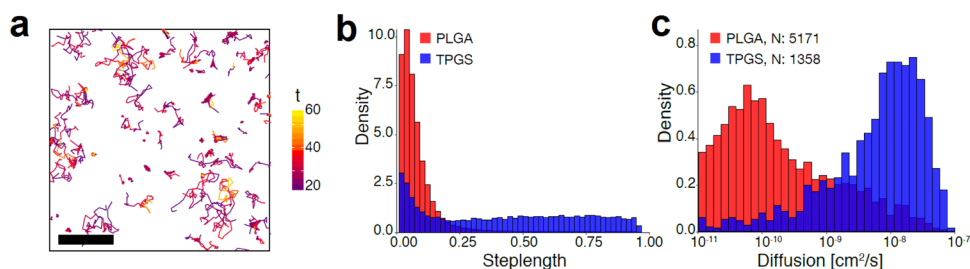


Figure 5. (a) Representative moving trajectories of nanoparticles at the boundary between the mucus and the bacterial outer membrane-mimicking the lipid bilayer obtained from tracking experiments (shown in Figure 2b, color code indicates the observation time); (b) distribution of the step size; (c) distributions of the effective diffusivities (D_{eff}). Red: PLGA nanoparticles (type I, Table S3); blue: TPGS–PLGA hybrid nanoparticles (type J, Table S3).

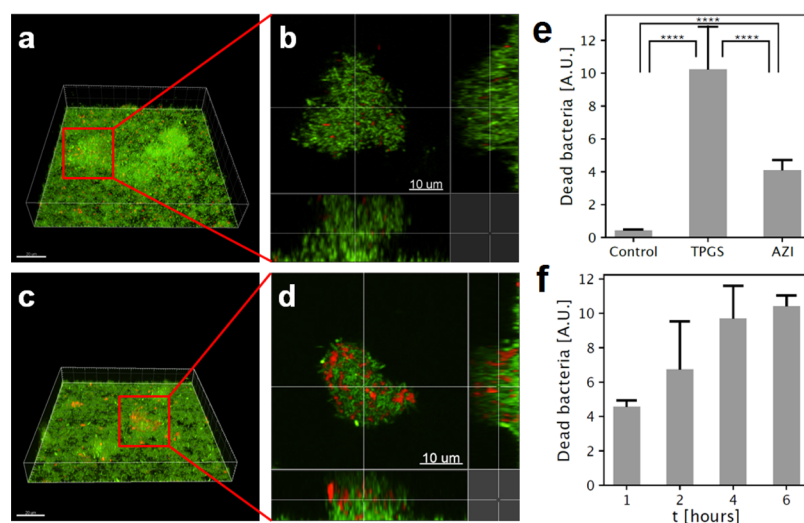


Figure 6. Killing efficacy of AZI and AZI-loaded TPGS–PLGA hybrid nanoparticles (type D, Table S4) against the *P. aeruginosa* biofilm (PAO1 tagged with GFP). The alive and dead *P. aeruginosa* bacteria appear green and red, respectively. (a,b) CLSM images of the *P. aeruginosa* biofilm treated with AZI at 6 h. (c,d) CLSM images of the *P. aeruginosa* biofilm treated with AZI-loaded TPGS–PLGA hybrid nanoparticles at 6 h. The alive and dead *P. aeruginosa* bacteria appear green and red, respectively. Scale bars: 10 μm . (e) Quantification of the relative killing efficiency of AZI and AZI-loaded TPGS–PLGA hybrid nanoparticles against the *P. aeruginosa* biofilm. Control group: the *P. aeruginosa* biofilm was only treated with PI. (f) Time dependency of the killing efficiency of AZI-loaded TPGS–PLGA hybrid nanoparticles. Error bars indicate error of the mean ($N = 3, 14$ and 11 for control, TPGS, and AZI, respectively). Statistics by student's *t*-test: **** indicate *p*-value < 0.0001.

Figure S5), though both nanoparticles demonstrated decreased accumulation in the biofilm at 24 h, suggesting that TPGS coating did not promote the escape of nanoparticles from the biofilm. This observation indirectly supports our expectation that TPGS could be cleaved by esterase produced by *P. aeruginosa* bacteria, thus leading to the surface-switching property of TPGS–PLGA hybrid nanoparticles and allowing the “decayed” nanoparticles for anchoring in the biofilm.

In summary, the TPGS–PLGA hybrid nanoparticles present hydrophilic surfaces with slight negative charges, which offer superior ability to penetrate through mucus and into the deeper layer of bacterial biofilms. Once localized in the biofilms, and the TPGS shell of the nanoparticles is cleaved into PEG and vitamin E, resulting in a lipophilic vitamin E-enriched surface of nanoparticles; this further promotes the accumulation of nanoparticles in the biofilms.

Killing Efficacy against Biofilm-Forming *P. aeruginosa*. The therapeutic efficacy of AZI in CF patients has been proven in many clinical trials,^{48–50} though it is not yet approved for the treatment of CF. In light of the promising findings, we employed AZI as an antimicrobial agent to investigate the antibiofilm efficacy of AZI-loaded TPGS–PLGA hybrid nanoparticles against CF-related *P. aeruginosa* biofilms. The MIC of AZI in solution for planktonic *P. aeruginosa* was determined to be 512 $\mu\text{g}/\text{mL}$, which is consistent with the early reports.²⁹ In our previous study, encapsulation of AZI in TPGS–PLGA hybrid nanoparticles increased the effect of AZI on prevention and eradication of *P. aeruginosa* biofilms due to the inhibition of quorum sensing-associated virulence factors (e.g., decrease the bacterial swarming motility and the production of pyocyanin and pyoverdinin).⁵¹

The nanoparticle-mediated killing efficacy against biofilm-forming *P. aeruginosa* was investigated by using the flow-chamber system by comprising the effects of shear stress and clearance. *P. aeruginosa* biofilms preformed in the flow-chamber system were treated with AZI and AZI-loaded

TPGS–PLGA hybrid nanoparticles, followed by staining with PI (specifically stain the dead bacterial cells⁵²). The killing efficacy was evaluated by using the fluorescent intensity (red color) of dead bacterial cells in the CLSM images. As observed in CLSM images, *P. aeruginosa* biofilms treated with AZI-loaded TPGS–PLGA hybrid nanoparticles presented more dead bacterial cells (red) than those treated with AZI (Figure 6a–d). Quantitative analysis of CLSM images demonstrated that AZI-loaded TPGS–PLGA hybrid nanoparticles presented approximately 2.5 times higher killing efficacy than AZI at 6 h (Figure 6e). Meanwhile, the effect of PI on the bacterial biofilms was only subtle within the investigating time (6 h). The enhanced killing efficacy could mainly be attributed to the fact that TPGS–PLGA hybrid nanoparticles promote the site-specific delivery of AZI and increase the drug concentration in the close proximity of the biofilm-forming bacteria. In addition, it should be noted that vitamin E released from the enzymatic hydrolysis of TPGS, as a well-known antioxidant, could also contribute to improving the susceptibility of *P. aeruginosa* to antimicrobial therapeutics and delaying the development of antimicrobial resistance.^{53,54} In addition, AZI nanoparticle formulation displayed a time-dependent killing efficacy (Figure 6f). This time-dependent killing efficacy could result from the sustained release behavior of the AZI-loaded nanoparticles formulation (Supporting Information, Figure S6).⁵⁵ It is worth to mention that, in previous studies, the beneficial effects on CF patients treated with AZI in solution have been demonstrated only up to 6 months, while longer durations of treatment resulted in reduced efficacy probably due to the emergence of antibiotic tolerant *P. aeruginosa* subpopulations.^{29,56} The sustained drug release from the TPGS–PLGA hybrid nanoparticles can provide a steady drug pharmacokinetic/pharmacodynamic profile for prolonged periods and thus may represent a promising approach to prevent the emergence of antibiotic tolerant *P. aeruginosa* subpopulations.^{3,57}

CONCLUSIONS

In conclusion, we demonstrate that ultrasmall TPGS–PLGA hybrid nanoparticles can potentially adapt to the complicated pathological environment in lungs of CF patients and achieve the site-specific delivery of antibiotics into bacterial biofilms. The TPGS–PLGA hybrid nanoparticles present the superior ability to penetrate through the mucus and accumulate into the interior of *P. aeruginosa* biofilms. As a consequence, encapsulation of AZI into TPGS–PLGA hybrid nanoparticles promotes the killing efficacy against biofilm-forming *P. aeruginosa* bacteria in a time-dependent manner. We, therefore, propose that TPGS–PLGA hybrid antimicrobial nanoparticles could improve the treatment of CF-related bacterial biofilm infections.

ASSOCIATED CONTENT

Supporting Information

The Supporting Information is available free of charge at <https://pubs.acs.org/doi/10.1021/acsami.9b19644>.

Synthesis and characterization of Atto655-conjugated PLGA; high-performance liquid chromatography with an evaporative light scattering detector (ELSD-HPLC); schematic representation of the Ripley's K function used for spatial point patterns; CLSM images of *P. aeruginosa* (PAO1) biofilms treated with DiIC₁₈₍₃₎-labeled nanoparticles; in vitro release profile of AZI from AZI-loaded TPGS–PLGA hybrid nanoparticles; composition of the growth medium for *P. aeruginosa* biofilm cultured in the flow-chamber system; preparation parameters, size, PDI, and zeta potential of PLGA nanoparticles, TPGS–PLGA hybrid nanoparticles, and fluorescent nanoparticles; and preparation and characterization of AZI-loaded TPGS–PLGA hybrid nanoparticles (PDF)

AUTHOR INFORMATION

Corresponding Authors

*E-mail: hatzakis@nano.ku.dk (N.H.).

*E-mail: hanne.morck@sund.ku.dk (H.M.N.).

ORCID

Feng Wan: 0000-0003-2822-9029

Søren S.-R. Bohr: 0000-0002-8107-2465

Tommy Nylander: 0000-0001-9420-2217

Mikkel Boas Thygesen: 0000-0002-0158-2802

Knud Jørgen Jensen: 0000-0003-3525-5452

Nikos Hatzakis: 0000-0003-4202-0328

Hanne Mørck Nielsen: 0000-0002-7285-9100

Notes

The authors declare no competing financial interest.

ACKNOWLEDGMENTS

This work was funded by the Danish Council for Independent Research, Technology and Production Sciences (DFR-4093-00062) (F.W.), Lundbeck Foundation (R264-2017-3404) (F.W.), and the University of Copenhagen 2016 Programme of Excellence Research Centre for Control of Antibiotic Resistance (UC-CARE) (S.N.K.). H.M.N. acknowledges funding from Novo Nordisk Foundation (Grand Challenge Program; NNF16OC0021948). N.H. acknowledges funding from Villum Young Investigator program (grant 10099) and the Carlsberg foundation distinguished Associate Professor Program (CF16-0797).

REFERENCES

- (1) Govan, J. R.; Deretic, V. Microbial Pathogenesis in Cystic Fibrosis: Mucoid *Pseudomonas Aeruginosa* and *Burkholderia Cepacia*. *Microbiol. Mol. Biol. Rev.* **1996**, *60*, 539–574.
- (2) Lechtzin, N.; John, M.; Irizarry, R.; Merlo, C.; Diette, G. B.; Boyle, M. P. Outcomes of Adults with Cystic Fibrosis Infected with Antibiotic-resistant *Pseudomonas Aeruginosa*. *Respiration* **2006**, *73*, 27–33.
- (3) Ciofu, O.; Tolker-Nielsen, T.; Jensen, P. Ø.; Wang, H.; Høiby, N. Antimicrobial Resistance, Respiratory Tract Infections and Role of Biofilms in Lung Infections in Cystic Fibrosis Patients. *Adv. Drug Delivery Rev.* **2015**, *85*, 7–23.
- (4) Geller, D. E.; Pitlick, W. H.; Nardella, P. A.; Tracewell, W. G.; Ramsey, B. W. Pharmacokinetics and Bioavailability of Aerosolized Tobramycin in Cystic Fibrosis. *Chest* **2002**, *122*, 219–226.
- (5) Gibson, R. L.; Retsch-Bogart, G. Z.; Oermann, C.; Milla, C.; Pilewski, J.; Daines, C.; Ahrens, R.; Leon, K.; Cohen, M.; McNamara, S.; Callahan, T. L.; Markus, R.; Burns, J. L. Microbiology, Safety, and Pharmacokinetics of Aztreonam lysinate for Inhalation in Patients with Cystic Fibrosis. *Pediatr. Pulmonol.* **2006**, *41*, 656–665.
- (6) Dudley, M. N.; Loutit, J.; Griffith, D. C. Aerosol Antibiotics: Considerations in Pharmacological and Clinical evaluation. *Curr. Opin. Biotechnol.* **2008**, *19*, 637–643.
- (7) Fahy, J. V.; Dickey, B. F. Airway Mucus Function and Dysfunction. *N. Engl. J. Med.* **2010**, *363*, 2233–2247.
- (8) Treacy, K.; Tunney, M.; Elborn, J. S.; Bradley, J. M. Mucociliary Clearance in Cystic Fibrosis: Physiology and Pharmacological Treatments. *Paediatr. Child Health* **2011**, *21*, 425–430.
- (9) Flemming, H.-C.; Wingender, J. The Biofilm Matrix. *Nat. Rev. Microbiol.* **2010**, *8*, 623–633.
- (10) Costerton, J. W.; Stewart, P. S.; Greenberg, E. P. Bacterial Biofilms: A Common Cause of Persistent Infections. *Science* **1999**, *284*, 1318–1322.
- (11) Huh, A. J.; Kwon, Y. J. “Nanoantibiotics”: A New Paradigm for Treating Infectious Diseases using Nanomaterials in the Antibiotics Resistant Era. *J. Controlled Release* **2011**, *156*, 128–145.
- (12) Forier, K.; Raemdonck, K.; De Smedt, S. C.; Demeester, J.; Coenye, T.; Braeckmans, K. Lipid and Polymer Nanoparticles for Drug Delivery to Bacterial Biofilms. *J. Controlled Release* **2014**, *190*, 607–623.
- (13) García-Díaz, M.; Birch, D.; Wan, F.; Nielsen, H. M. The Role of Mucus as An Invisible Cloak to Transepithelial Drug Delivery by Nanoparticles. *Adv. Drug Delivery Rev.* **2018**, *124*, 107–124.
- (14) Forier, K.; Messiaen, A.-S.; Raemdonck, K.; Nelis, H.; De Smedt, S.; Demeester, J.; Coenye, T.; Braeckmans, K. Probing the Size Limit for Nanomedicine Penetration into *Burkholderia Multivorans* and *Pseudomonas Aeruginosa* Biofilms. *J. Controlled Release* **2014**, *195*, 21–28.
- (15) Suk, J. S.; Lai, S. K.; Wang, Y.-Y.; Ensign, L. M.; Zeitlin, P. L.; Boyle, M. P.; Hanes, J. The Penetration of Fresh Undiluted Sputum Expectorated by Cystic Fibrosis Patients by Non-adhesive Polymer Nanoparticles. *Biomaterials* **2009**, *30*, 2591–2597.
- (16) Liu, Y.; Busscher, H. J.; Zhao, B.; Li, Y.; Zhang, Z.; van der Mei, H. C.; Ren, Y.; Shi, L. Surface-Adaptive, Antimicrobially Loaded, Micellar Nanocarriers with Enhanced Penetration and Killing Efficiency in Staphylococcal Biofilms. *ACS Nano* **2016**, *10*, 4779–4789.
- (17) Radovic-Moreno, A. F.; Lu, T. K.; Puscasu, V. A.; Yoon, C. J.; Langer, R.; Farokhzad, O. C. Surface Charge-Switching Polymeric Nanoparticles for Bacterial Cell Wall-Targeted Delivery of Antibiotics. *ACS Nano* **2012**, *6*, 4279–4287.
- (18) Horev, B.; Klein, M. I.; Hwang, G.; Li, Y.; Kim, D.; Koo, H.; Benoit, D. S. W. pH-activated Nanoparticles for Controlled Topical Delivery of Farnesol to Disrupt Oral Biofilm Virulence. *ACS Nano* **2015**, *9*, 2390–2404.
- (19) Tate, S.; MacGregor, G.; Davis, M.; Innes, J.; Greening, A. Airways in Cystic Fibrosis are Acidified: Detection by Exhaled Breath Condensate. *Thorax* **2002**, *57*, 926–929.

- (20) Poschet, J.; Perket, E.; Deretic, V. Hyperacidification in Cystic Fibrosis: Links with Lung Disease and New Prospects for Treatment. *Trends Mol. Med.* **2002**, *8*, 512–519.
- (21) Bodem, C. R.; Lampton, L. M.; Miller, D. P.; Tarka, E. F.; Everett, E. D. Endobronchial pH. *Am. Rev. Respir. Dis.* **1983**, *127*, 39–41.
- (22) Smith, J. J.; Travis, S. M.; Greenberg, E. P.; Welsh, M. J. Cystic Fibrosis Airway Epithelia Fail to Kill Bacteria Because of Abnormal Airway Surface Fluid. *Cell* **1996**, *85*, 229–236.
- (23) Zhang, Z.; Tan, S.; Feng, S.-S. Vitamin E TPGS as A Molecular Biomaterial for Drug Delivery. *Biomaterials* **2012**, *33*, 4889–4906.
- (24) Guo, Y.; Luo, J.; Tan, S.; Otieno, B. O.; Zhang, Z. The Applications of Vitamin E TPGS in Drug Delivery. *Eur. J. Pharm. Sci.* **2013**, *49*, 175–186.
- (25) Dahe, G. J.; Kadam, S. S.; Sabale, S. S.; Kadam, D. P.; Sarkate, L. B.; Bellare, J. R. In vivo Evaluation of the Biocompatibility of Surface Modified Hemodialysis Polysulfone Hollow Fibers in Rat. *PLoS One* **2011**, *6*, No. e25236.
- (26) Tielen, P.; Rosenau, F.; Wilhelm, S.; Jaeger, K.-E.; Flemming, H.-C.; Wingender, J. Extracellular Enzymes Affect Biofilm Formation of Mucoid *Pseudomonas Aeruginosa*. *Microbiology* **2010**, *156*, 2239–2252.
- (27) Koziróg, A.; Otlewska, A.; Brycki, B. Viability, Enzymatic and Protein Profiles of *Pseudomonas aeruginosa* Biofilm and Planktonic Cells after Monomeric/Gemini Surfactant Treatment. *Molecules* **2018**, *23*, 1294.
- (28) Lai, S. K.; Wang, Y.-Y.; Hanes, J. Mucus-penetrating Nanoparticles for Drug and Gene Delivery to Mucosal Tissues. *Adv. Drug Delivery Rev.* **2009**, *61*, 158–171.
- (29) Imperi, F.; Leoni, L.; Visca, P. Antivirulence Activity of Azithromycin in *Pseudomonas Aeruginosa*. *Front. Microbiol.* **2014**, *5*, 178.
- (30) Kim, Y.; Lee Chung, B.; Ma, M.; Mulder, W. J. M.; Fayad, Z. A.; Farokhzad, O. C.; Langer, R. Mass Production and Size Control of Lipid-polymer Hybrid Nanoparticles through Controlled Microvortices. *Nano Lett.* **2012**, *12*, 3587–3591.
- (31) Boegh, M.; Baldursdóttir, S. G.; Müllertz, A.; Nielsen, H. M. Property Profiling of Biosimilar Mucus in a Novel Mucus-containing in vitro Model for Assessment of Intestinal Drug Absorption. *Eur. J. Pharm. Biopharm.* **2014**, *87*, 227–235.
- (32) Cremer, P. S.; Boxer, S. G. Formation and Spreading of Lipid Bilayers on Planar Glass Supports. *J. Phys. Chem. B* **1999**, *103*, 2554–2559.
- (33) Strömstedt, A. A.; Ringstad, L.; Schmidtchen, A.; Malmsten, M. Interaction Between Amphiphilic Peptides and Phospholipid Membranes. *Curr. Opin. Colloid Interface Sci.* **2010**, *15*, 467–478.
- (34) Tinevez, J.-Y.; Perry, N.; Schindelin, J.; Hoopes, G. M.; Reynolds, G. D.; Laplantine, E.; Bednarek, S. Y.; Shorte, S. L.; Eliceiri, K. W. TrackMate: An Open and Extensible Platform for Single-particle Tracking. *Methods* **2017**, *115*, 80–90.
- (35) Lowe, D. G. Distinctive Image Features from Scale-Invariant Keypoints. *Int. J. Comput. Vis.* **2004**, *60*, 91–110.
- (36) Bretzner, L.; Lindeberg, T. Feature Tracking with Automatic Selection of Spatial Scales. *Comput. Vis. Image Understand.* **1998**, *71*, 385–392.
- (37) Ripley, B. D. The Second-Order Analysis of Stationary Point Processes. *J. Appl. Probab.* **1976**, *13*, 255–266.
- (38) Konopka, M. C.; Weisshaar, J. C. Heterogeneous Motion of Secretory Vesicles in the Actin Cortex of Live Cells: 3D Tracking to 5-nm Accuracy. *J. Phys. Chem. A* **2004**, *108*, 9814–9826.
- (39) Rocha, S.; Hutchison, J. A.; Peneva, K.; Herrmann, A.; Müllen, K.; Skjöt, M.; Jørgensen, C. I.; Svendsen, A.; De Schryver, F. C.; Hofkens, J.; Uji-i, H. Linking Phospholipase Mobility to Activity by Single-molecule Wide-field Microscopy. *ChemPhysChem* **2009**, *10*, 151–161.
- (40) Dahan, M.; Lévi, S.; Luccardini, C.; Rostaing, P.; Riveau, B. a.; Triller, A. Diffusion Dynamics of Glycine Receptors Revealed by Single-quantum Dot Tracking. *Science* **2003**, *302*, 442–445.
- (41) Weiss Nielsen, M.; Sternberg, C.; Molin, S.; Regenber, B. *Pseudomonas Aeruginosa* and *Saccharomyces Cerevisiae* Biofilm in Flow Cells. *J. Visualized Exp.* **2011**, *47*, 2383.
- (42) Haagen, J. A. J.; Klausen, M.; Ernst, R. K.; Miller, S. I.; Folkesson, A.; Tolker-Nielsen, T.; Molin, S. Differentiation and Distribution of Colistin- and Sodium Dodecyl Sulfate-Tolerant Cells in *Pseudomonas aeruginosa* Biofilms. *J. Bacteriol.* **2006**, *189*, 28–37.
- (43) Kim, Y.; Fay, F.; Cormode, D. P.; Sanchez-Gaytan, B. L.; Tang, J.; Hennessy, E. J.; Ma, M.; Moore, K.; Farokhzad, O. C.; Fisher, E. A.; Mulder, W. J. M.; Langer, R.; Fayad, Z. A. Single Step Reconstitution of Multifunctional High-Density Lipoprotein-Derived Nanomaterials Using Microfluidics. *ACS Nano* **2013**, *7*, 9975–9983.
- (44) Valencia, P. M.; Basto, P. A.; Zhang, L.; Rhee, M.; Langer, R.; Farokhzad, O. C.; Karnik, R. Single-step Assembly of Homogenous Lipid-polymeric and Lipid-quantum Dot Nanoparticles Enabled by Microfluidic Rapid Mixing. *ACS Nano* **2010**, *4*, 1671–1679.
- (45) Aucamp, M.; Odendaal, R.; Liebenberg, W.; Hamman, J. Amorphous Azithromycin with Improved Aqueous Solubility and Intestinal Membrane Permeability. *Drug Dev. Ind. Pharm.* **2015**, *41*, 1100–1108.
- (46) Wan, F.; Nylander, T.; Klodzinska, S. N.; Foged, C.; Yang, M.; Baldursdóttir, S. G.; Nielsen, H. M. Lipid Shell-Enveloped Polymeric Nanoparticles with High Integrity of Lipid Shells Improve Mucus Penetration and Interaction with Cystic Fibrosis-Related Bacterial Biofilms. *ACS Appl. Mater. Interfaces* **2018**, *10*, 10678–10687.
- (47) Klausen, M.; Aaes-Jørgensen, A.; Molin, S.; Tolker-Nielsen, T. Involvement of Bacterial Migration in the Development of Complex Multicellular Structures in *Pseudomonas aeruginosa* Biofilms. *Mol. Microbiol.* **2003**, *50*, 61–68.
- (48) Wolter, J.; Seeney, S.; Bell, S.; Bowler, S.; Masel, P.; McCormack, J. Effect of Long Term Treatment with Azithromycin on Disease Parameters in Cystic Fibrosis: a Randomised Trial. *Thorax* **2002**, *57*, 212–216.
- (49) Saiman, L.; Marshall, B. C.; Mayer-Hamblett, N.; Burns, J. L.; Quittner, A. L.; Cibene, D. A.; Coquillotte, S.; Fieberg, A. Y.; Accurso, F. J. Azithromycin in Patients With Cystic Fibrosis Chronically Infected With *Pseudomonas aeruginosa*. *JAMA* **2003**, *290*, 1749–1756.
- (50) Jaffé, A.; Francis, J.; Rosenthal, M.; Bush, A. Long-term Azithromycin May Improve Lung Function in Children with Cystic Fibrosis. *Lancet* **1998**, *351*, 420.
- (51) Klodzińska, S. N.; Wan, F.; Jumaa, H.; Sternberg, C.; Rades, T.; Nielsen, H. M. Utilizing Nanoparticles for Improving Anti-biofilm Effects of Azithromycin: A Head-to-head Comparison of Modified Hyaluronic Acid Nanogels and Coated Poly (lactic-co-glycolic acid) Nanoparticles. *J. Colloid Interface Sci.* **2019**, *555*, 595–606.
- (52) Pamp, S. J.; Gjermansen, M.; Johansen, H. K.; Tolker-Nielsen, T. Tolerance to the Antimicrobial Peptide Colistin in *Pseudomonas aeruginosa* Biofilms is Linked to Metabolically Active Cells, and Depends on the pmr and mexAB-oprM Genes. *Mol. Microbiol.* **2008**, *68*, 223–240.
- (53) Høiby, N. Understanding Bacterial Biofilms in Patients with Cystic Fibrosis: Current and Innovative Approaches to Potential Therapies. *J. Cystic Fibrosis* **2002**, *1*, 249–254.
- (54) Constantinou, C.; Papas, A.; Constantinou, A. I. Vitamin E and Cancer: An Insight into the Anticancer Activities of Vitamin E Isomers and Analogs. *Int. J. Cancer* **2008**, *123*, 739–752.
- (55) Danhier, F.; Ansorena, E.; Silva, J. M.; Coco, R.; Le Breton, A.; Préat, V. PLGA-based Nanoparticles: An Overview of Biomedical Applications. *J. Controlled Release* **2012**, *161*, 505–522.
- (56) Fleet, J. E.; Guha, K.; Piper, S.; Banya, W.; Bilton, D.; Hodson, M. E. A Retrospective Analysis of the Impact of Azithromycin Maintenance Therapy on Adults Attending a UK Cystic Fibrosis Clinic. *J. Cystic Fibrosis* **2013**, *12*, 49–53.
- (57) Levy, S. B.; Marshall, B. Antibacterial Resistance Worldwide: Causes, Challenges and Responses. *Nat. Med.* **2004**, *10*, S122–S129.